

Observation of kidney microstructure by X-ray CT

Naoki Kunishima*

Abstract

The nano3DX from Rigaku is a laboratory-based X-ray microscope that enables nondestructive observation of three-dimensional structures of a sample by CT reconstruction from X-ray projection images. As an example of biological applications of laboratory-based X-ray microscopy, the X-ray CT observation of kidney microstructure has been performed. By observing mouse kidney sections stained with heavy-element reagents and resin-embedded in sheet form, a three-dimensional rendering of nephrons, the functional units of the kidney, has been obtained successfully at micron-level spatial resolution. Furthermore, a detailed statistical analysis of CT images from five independent nephrons showed that heavy-element-stained proximal and distal tubules can be distinguished by brightness values. Future developments in laboratory-based X-ray microscopy are expected to include applications in medicine and structural biology.

1. Introduction

X-ray microscopy is an imaging technique that uses the high penetrability of X-rays to nondestructively observe the interior of thick samples. Consecutive projection images taken by an X-ray microscope are processed by a computational method called Computed Tomography (CT) to reconstruct a three-dimensional (3D) image, resulting in a nondestructive observation of 3D structures. The nano3DX from Rigaku is a laboratory-based X-ray microscope that utilizes a user-friendly laboratory X-ray source⁽¹⁾. X-ray CT methods using laboratory-based X-ray microscopes have been widely applied to industrial materials⁽²⁾, for instance, and recently to some biological samples^{(3)–(5)}. In this paper, as an example of biological applications, we introduce the observation of microstructure of mouse kidney using nano3DX⁽⁵⁾.

2. Overview of nano3DX

Features of nano3DX are shown in Fig. 1. The main body of the device is about as tall as a person. An observation sample is mounted on the central sample stage, X-rays are irradiated from the left side, and transmitted X-rays through the sample are captured by the camera on the right side. In the camera, the transmitted X-rays are converted into light by the scintillator, which is then imaged onto the sensor surface of the photo-detector by an optical lens. Because this system adopts the quasi-parallel geometry that takes images with short sample-detector distances, we can reduce defects from thermal fluctuation of the light source compared to conventional cone-beam X-ray microscopes with geometrical magnification, thereby enabling a micron or submicron level of high-resolution observations⁽¹⁾. Please refer to separate reports for a general review of the theoretical background⁽⁶⁾ and

biological applications^{(7),(8)} of X-ray microscopy. Here we briefly describe the observation of bio-specimens.

Since bio-specimens are composed mainly of light elements, observing them usually involves problems from low image contrast. To obtain contrast, it is first important to select X-rays with appropriate wavelengths so that X-rays transmitted through the observation sample are moderately absorbed by it. The nano3DX system uses a method of selecting characteristic and continuous X-rays with different wavelengths from four different targets (Cr, Cu, Mo, and W). For most observations of bio-specimens, either Cu or Mo targets are used because they provide better contrast. The attainable contrast can be evaluated by taking a projection image. The area of interest in the sample should transmit 50–90% of the incident X-rays. Points to be considered in the case of inadequate contrast are wavelength selection, sample size adjustment by trimming, and various contrast enhancements. For example, contrast enhancement is possible through image processing, of which phase retrieval^{(9),(10)} is a representative technique. Phase retrieval is applicable to unstained bio-specimens, and an example of a 3D rendering of embryos within live pansy seeds⁽³⁾ from observations using phase retrieval has been reported. On the other hand, contrast can be enhanced by experimental techniques. For example, as applied to the mouse kidney sample presented here, staining with appropriate reagents containing heavy elements enhances the absorption contrast of bio-specimens. Contrast can also be enhanced by replacing the water in the unstained bio-specimens with paraffin or other materials with higher X-ray transmittance, and a 3D observation of glomeruli in a paraffin-embedded mouse kidney⁽⁴⁾ has been reported.

* X-ray Research Laboratory, Rigaku Corporation



Fig. 1. Laboratory-based X-ray microscope, nano3DX. External appearance (left) and region around sample stage (right).

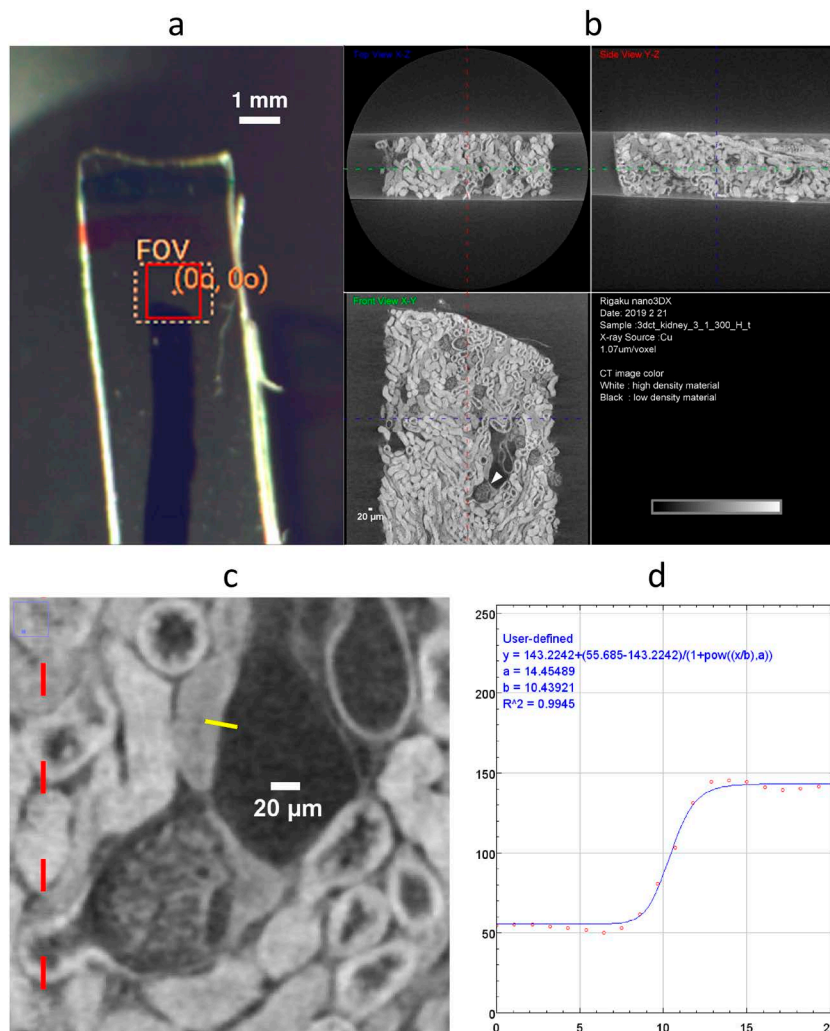


Fig. 2. Observation of mouse kidney sample using nano3DX. This figure was taken from Ref. 5. (a) Experiment set-up, (b) CT slices from three orthogonal perspectives, (c) partial enlargement around a renal corpuscle indicated by an arrowhead in (b), and (d) evaluation of spatial resolution from a brightness profile (abscissa and ordinate denote length and 256 grayscale brightness values, respectively) along a yellow line (about $20\ \mu\text{m}$) in (c). (a–c) and (d) were prepared using the nano3DX software and the software *ImageJ*, respectively.

3. Observation of Mouse Kidney Sample Using nano3DX

As an example of biological applications of laboratory-based X-ray microscopy, the X-ray CT observation of kidney microstructure⁽⁵⁾ has been performed. An overview of the observation is shown in Fig. 2. Samples for nano3DX observation were prepared by sectioning mouse kidney samples into 1 mm wide and 0.3 mm thick sections, staining them with osmium tetroxide (OsO_4), which is commonly used in electron microscopy as a heavy-element reagent, and then embedding them in Epon resin, also used in electron microscopy, in a sheet form (Fig. 2a). A projection data set consisting of 800 frames was captured using X-rays from a Cu-target with a pixel size of $1.1 \mu\text{m}$ and an exposure time of 20 seconds per frame. The field of view was 1.3 mm, thereby covering the width of the sample. The X-ray transmission rate was 72%. As a result of CT reconstruction, a high-contrast visualization of mouse kidney microstructure was achieved due to the contrast-enhancing effect of the Os staining (Fig. 2b, c). The blur width of the brightness profile along a straight line perpendicular to the boundary between tissue and resin was measured as $1.6 \mu\text{m}$, indicating that high spatial resolution close to the limit due to the pixel size was obtained.

4. 3D Rendering of a Single Nephron

The functional unit of the kidney is called the nephron, which comprises a renal corpuscle producing primary urine from blood and a renal tubule producing urine from the primary urine. The tubule in a single nephron of a mouse originates in a single renal corpuscle and runs over 10 mm to the collecting duct. In the CT slice magnification shown in Fig. 2c, the black circular object on the lower left is the renal corpuscle, which is surrounded by intricately curved tubules. Since clear CT images were obtained in this observation, we attempted to extract a single nephron (Fig. 3). First, the image analysis software *ImageJ* was used to identify the region containing the renal corpuscle and the tubule belonging to it in each CT slice (Fig. 4a), then a mask specifying the region (Fig. 4b) was manually created, and a CT slice containing only a single nephron (Fig. 4c) was created by multiplying the mask with the original CT slice. The CT slices were integrated by the stereoscopic display software *Drishti*, and a single nephron of a mouse kidney was finally visualized in 3D (Fig. 3). This single nephron model includes the proximal tubule (PT) originating from the renal corpuscle (RC), the distal tubule (DT) returning to RC through an interruption indicated by a dotted line in the figure, and the terminal collecting duct (CD) (Fig. 3b), and also includes the vasculature system consisting of the afferent arteriole (AA), which enters RC from the larger artery, the efferent artery (EA), which branches off immediately after exiting through the glomerulus (GM), a tuft of capillaries within RC (Fig. 3a). On the vascular pole side of GM, there is the macula densa (MD), which

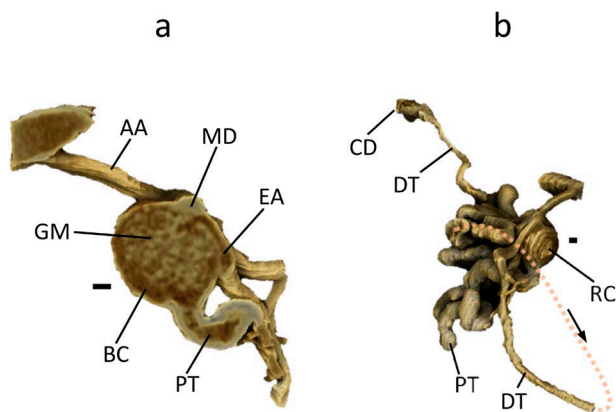


Fig. 3. 3D rendering of single nephron of mouse kidney.

This figure was taken from Ref. 5 and was prepared using the software *Drishti*. (a) Cross-section of the renal corpuscle, and (b) entire view of the nephron. Scale bars represent $20 \mu\text{m}$. Abbreviation for each part is annotated in the text.

communicates with DT, whereas on the tubular pole side, there is a region called Bowman's capsule (BC) that collects primary urine (Fig. 3a). These structures are consistent with previously studied mouse nephron findings, but differ in that they have been visualized in 3D detail. The length of the tubule in the current model was measured to be 4 mm. Thus, up to 40% of the total length of the single nephron was modeled.

5. Image Analysis of Tubules

We then tried a feature extraction by image analysis based on the micron-level CT images of mouse kidneys obtained by laboratory-based X-ray microscopy (Fig. 4). The tubules include the proximal tubule (PT), which begins in the renal corpuscle and is located upstream, and the distal tubule (DT) located downstream. Observation of PT and DT revealed that there appeared to be a difference in CT brightness values between the two. We therefore compared CT brightness histograms (the abscissa represents brightness value) in the following three ways: the CT slice including entire tubules (Fig. 4d, g), from which PT (Fig. 4e, h) and DT (Fig. 4f, i), both of which belong to the same nephron, were cut out. In Fig. 4d–i, brightness values are displayed in a color scale. In the histogram of brightness values, the histogram of entire tubules is overlaid in gray to clarify the relative positions of brightness peaks. The resulting brightness histograms showed clearly different peak positions between PT and DT. A more detailed statistical analysis of CT images of five independent nephrons showed that the heavy-element-stained PT and DT could be distinguished by their brightness values; i.e., the difference in mean brightness values was significant (Table 1). In the table, CNR stands for contrast-to-noise ratio and is defined as the ratio of the difference in mean CT brightness values between two 5-pixel square regions of comparison in a CT slice to the standard deviation of differences. Air-PT CNR and Air-DT CNR were calculated from the mean CT

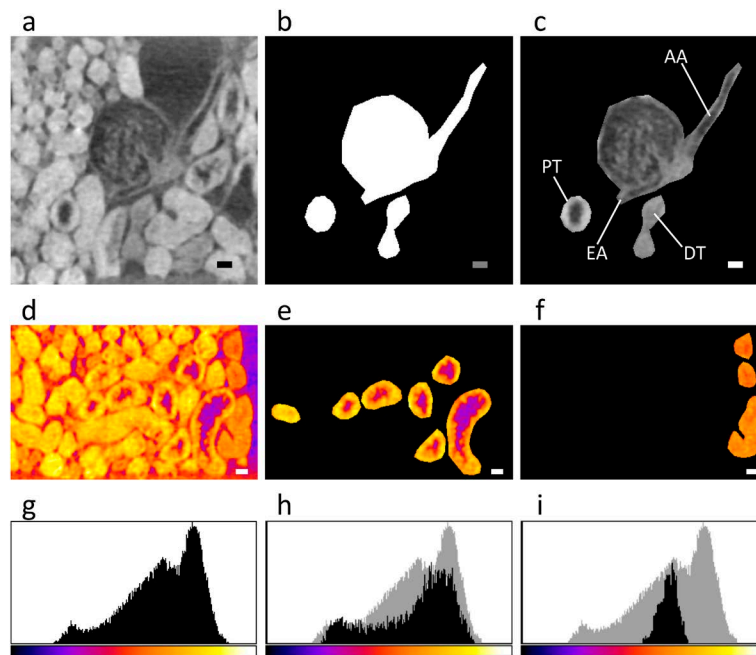


Fig. 4. Image analysis of tubules of mouse kidney. This figure was taken from Ref. 5 and was prepared using the software *ImageJ*. Scale bars represent $20\mu\text{m}$. (a) a part of CT slice around a renal corpuscle, (b) a mask that specifies regions belonging to the same nephron in the slice, and (c) regions of the single nephron extracted using the mask. Abbreviation for each part is the same as that in Fig. 3. Image analysis of tubules through a comparison between CT slices (d–f) and corresponding histograms of brightness values (g–i) is presented. See text for details.

Table 1. Statistical analysis of CT brightness values. Adapted from Ref.5.

Air-PT CNR	Air-DT CNR	<i>p</i> -Value
45.2 ± 2.3	32.1 ± 2.0	3.4×10^{-5}

brightness values measured in the paired regions of air and proximal tubular cortex, and air and distal tubular cortex, respectively. These CNRs were calculated for five independent nephrons and are given in the table as 95% confidence intervals of estimated population mean values. The difference between the mean values of Air-PT and Air-DT CNRs was evaluated by Student's *t*-test, and the resulting *p*-value is given in the table. The osmium reagent used for staining kidney samples in this study is known to have a high affinity for fatty acids containing unsaturated bonds, for instance ⁽¹¹⁾. The difference in CT brightness values may have been caused by the difference in affinity for the osmium reagent in proximal and distal tubules.

6. Conclusion

The mouse kidney sections observed in this study using an X-ray microscope were prototyped to mimic common specimens used in renal biopsies. Taking advantage of the nondestructive nature of X-ray microscopy, it is possible for the same sample to be observed in detail by electron microscopy after the X-ray observation. Therefore, further development of this method may contribute to more advanced

pathological diagnosis of renal biopsies, which is expected to provide useful methodology in medicine and structural biology as a future application of laboratory-based X-ray microscopy. At Rigaku Corporation, we are pioneering biological applications of nano3DX with a focus on medical use. Furthermore, we are developing an ultrahigh-resolution X-ray microscope for laboratory use at a level that enables observation of intracellular organelles, aiming to realize the seamless observation of bio-specimens through the complementary use of X-ray microscopy, optical microscopy, and electron microscopy. The seamless observation of hierarchical structure of organisms is a bottleneck of modern biology and is of critical importance.

References

- (1) *Rigaku Journal (Japanese version)*, **43** (2012), No. 2, 28–30.
- (2) Y. Takeda: *Rigaku Journal*, **35** (2019), No. 2, 18–21.
- (3) N. Kunishima, Y. Takeda, R. Hirose, D. Kalasová, J. Šalplachta and K. Omote: *Plant Methods*, **16** (2020) 7.
- (4) N. Kunishima, R. Hirose, Y. Takeda, K. Ito, K. Furuichi and K. Omote: *Sci. Rep.*, **12** (2022) 9436.
- (5) N. Kunishima, Y. Takeda, R. Hirose, S. Kume, M. Maeda, A. Oguchi, M. Yanagita, H. Shibuya, M. Tamura, Y. Kataoka, Y. Murakawa, K. Ito and K. Omote: *Microscopy*, **71** (2022) 315–323.
- (6) Y. Takeda and K. Hamada: *Rigaku Journal*, **31** (2015), No. 1, 10–15.
- (7) N. Kunishima: *Rigaku Journal*, **36** (2020), No. 1, 33–36.
- (8) N. Kunishima: *Medical Science Digest (Japanese)*, **48** (2022), No. 14, 26–29.
- (9) D. Paganin, S. C. Mayo, T. E. Gureyev, P. R. Miller and S. W.

- Wilkins: *J. Microscopy*, **206** (2002), 33–40.
- (10) D. Kalasová, T. Zikmund, L. Pina, Y. Takeda, M. Horváth, K. Omote and J. Kaiser: *IEEE Trans. Instrum. Measure.*, **69** (2020) 1170–1178.
- (11) J. A. Kiernan: *J. Histotechnol.*, **30** (2007) 87–106.